Preparation and Characterization of Nanocellulose Coating Modified by Titanium Dioxide

Yi Zhang,[a] Shengfei Yu,[a,*] and Wusheng Luo [b]

The hydrophilic character of cellulose nanowhiskers (CNWs) coating was changed by the use of TiO_2 to modify CNWs, thus preparing TiO_2/CNWs coating by a two-step method. Meanwhile, the effect of the additive amount and particle size of TiO_2 on the surface structure and water contact angle (WCA) of the coatings was studied. The solid contents of the suspension were characterized by Fourier infrared spectroscopy (FTIR), X-ray photoelectron spectroscopy (XPS), and X-ray diffraction (XRD). The TiO_2/CNWs coating was characterized *via* scanning electron microscopy (SEM) and atomic force microscopy (AFM). Moreover, their wettability by water was revealed by the contact angle analyzer. The AFM and WCA analyses showed different additive amount and particle size of TiO_2 have different effects on the surface structure and the WCA of the coatings. When the additive amount of TiO_2 was 0.2 wt.% and the particle size of TiO_2 was 30 nm, the WCA and surface roughness (R_q) of the obtained TiO_2/CNWs coating reached maximum values of 86.2° and 135nm, respectively. The TiO_2 was relatively evenly distributed in the coating and the addition of TiO_2 increased the crystallinity of CNWs from 79.67% to 84.89%. In addition, the FTIR and XPS analyses showed that TiO_2 only physically dispersed in CNWs instead of having significant chemical reaction with CNWs.

DOI: 10.15376/biores.17.1.504-518

Keywords: Cellulose nanowhiskers; TiO_2; Coating

*Contact information: a: College of Materials Science and Engineering, Central South University of Forestry and Technology, Changsha 410004, Hunan, P. R. China; b: College of Mechanical and Electrical Engineering, Central South University of Forestry and Technology, Changsha 410004, Hunan, P. R. China; * Corresponding author: yushengfei503@sina.com*

INTRODUCTION

Cellulose is the most widely distributed and abundant biomass material in nature. It is a long-chain polysaccharide polymer consisting of β-1-4-glycosidically-linked anhydroglucose units with three reactive hydroxyl groups per anhydroglucose unit. Nanocellulose can be obtained from plant cellulose by several processing methods such as the mechanical treatment, chemical treatment, enzymatic treatments, *etc*., and it possesses various forms, including cellulose nanowhiskers (CNWs), also known as nanocrystalline cellulose (NCC) and cellulose nanocrystals (CNCs), nanofibrillated cellulose (also called cellulose nanofibril (CNF)), and bacterial cellulose (BC) (Abitbol *et al.* 2016; Nguyen *et al.* 2019; Čolić *et al.* 2020; Zinge and Kandasubramanian 2020). Compared with other forms of nanocellulose, CNWs, as a whiskers form of nanocellulose, has better thermal stability, strength, *etc.* (Borsoi *et al.* 2016). Nanocellulose has been studied extensively in coatings, particularly in oxygen barrier and grease barrier coatings, due to its non-toxicity, non-pollution, biodegradability, high stiffness and tensile strength, facile modification, *etc.*

(Hubbe *et al.* 2017; Herrera *et al.* 2017; Xue *et al.* 2017). Although nanocellulose coating has excellent performance, it has its limitations (Tortorella *et al*. 2020). In particular, nanocellulose exhibits poor water resistance due to the copious hydrophilic hydroxyl groups in cellulose molecular chains. Nanocellulose coatings are relatively easy to be dissolved again in wet environments, and then the overall structure of the coating becomes destroyed, thereby restricting its application in high-humidity environments (Koppolu *et al*. 2019). Consequently, nanocellulose coatings need surface modifications to expand their applications. Modifications can be divided into two categories: organic and inorganic. Compared with organic modification (Zheng and Fu 2019), it is easy for inorganic modification to construct different microstructure of composite coatings, thus to change the hydrophilic or hydrophobic properties of coatings. Furthermore, coatings prepared by inorganic modifications generally possess better mechanical stability, acid and alkali resistance, and thermal stability. Huang *et al*. (2019) prepared a superhydrophobic cellulose nanocrystals (CNCs) /SiO_2 coatings by *in situ* growth of SiO_2. The obtained coatings showed excellent resistance to acid and alkali, and they retained their superhydrophobicity after sandpaper abrasion, finger-wipe, knife-scratch, and water-drip test. Wang *et al*. (2020) fabricated nanocellulose fiber (NCF)-composited superhydrophobic coating by using SiO_2 as the modifier. Notably, the coating remained superhydrophobic after over 360 cycles of grit abrasion. Ahmed *et al*. (2020) synthesized cellulose/graphene oxide nanocomposite (CGN) films by loading graphene oxide (GO) in a cellulose matrix. Compared with neat cellulose film, the CGN films rendered significant enhancement in the mechanical and thermal properties. Shi *et al*. (2020) prepared nano-graphene/copper/ cellulose composite coatings (NGCC) on flexible glass substrates by a spraying process. The tribological performance test of the NGCC indicated that adding a small amount of graphene/Cu improves the anti-wear property of cellulose. In addition, the particles size and particle contents can affect the surface structure and properties of materials or coatings in the modification. Lu *et al.* (2017) prepared fluoropolymer/SiO_2 composite coatings by adding different particle size of SiO_2 and found that the SiO_2 particles size had an obvious effect on the dispersive capacity and corrosion resistance coatings. Su *et al.* (2018) found the coatings fabricated by using nanoscale hydroxyapatite (HA) had lesser micro-crack and lower crack width than micron HA. Schütz *et al.* (2012) fabricated a nanofibrillated cellulose-TiO_2 hybrid film whose hardness and optical transmittance decreased towards high concentration of nanoparticles.

The most common inorganic modifier used to improve hydrophobicity of nanocellulose is SiO_2. Chen *et al*. (2020) loaded silica onto nanocellulose membranes through surface coating, followed by grafting hexadecyltrimethoxysilane groups (HDTMS). A small amount of SiO_2 distributed on the surface of the film gave the coating better hydrophobic property. Zuo *et al*. (2019) fabricated the aerogels of cellulose nanofibrils (CNF)/SiO_2. The combination of the chemical vapor deposition of fluorosilane reagent and the loaded SiO_2 nanoparticles gave rise to the superamphiphobic performance for nanocellulose-based aerogels, which achieved the contact angles of both the water and oil higher than 150°.

The superhydrophobic properties of above studies are achieved by combining low surface energy materials with the roughness constructed by loading SiO_2. At present, whether the solely constructure of roughness surface can achieve hydrophobicity or super-hydrophobicity is rarely studied. Nanocellulose coating is a hydrophilic substance, and the droplets present a Wenzel state on the surface of the coating, so increasing the roughness will increase its hydrophilic. However, the surface of nanocellulose constructed the micro-

nano mastoid structures by different methods to realize the transition from Wenzel state to Cassie state and finally led to hydrophobicity (Song and Rojas 2013).

The same as SiO_2, TiO_2 can change the hydrophilic or hydrophobic properties of cellulose materials or coatings. Kettunen *et al*. (2010) obtained hybrid TiO_2/nanocellulose aerogels by freeze-drying and chemical vapor deposition. In the stable state, hybrid TiO_2/nanocellulose aerogels shows water-repellent states which attributed to the formation of micro-nano structures. However, the missing roughness in microscale and nanoscale led to it showing water-superabsorbent states after UV illumination. Neelapala *et al*. (2017) successfully incorporated TiO_2 into cellulose acetate (CA) *via* phase inversion and then fabricated nanocomposite membranes. The addition of TiO_2 resulted in a decrease in finger-like projection and formed spongy structure, so the hydrophilicity of the CA membrane and the antifouling property significantly improved. Moreover, TiO_2 can endow nanocellulose coating with more additional properties due to its uniquely catalytic, chemically stable, light resistance, antibacterial and biocompatible properties (Ali *et al*. 2018). Galkina (2015) produced an antibacterial hybrid material for drug delivery applications by using TiO_2 chemically grafted onto cellulose nanofibers (CNF). Rathod *et al*. (2018) prepared nanocellulose/TiO_2 composites by ultrasonic impregnation method for photodegradation of mefenamic acid (MEF). Garusinghe *et al*. (2018) prepared a photocatalytic composite by using polyamide-amine-epichlorohydrin (PAE) as wet strength agent and a retention aid to embed TiO_2 nanoparticles (NPs) into the microfibrillated cellulose (MFC) matrix in a simple two-step mixing process. Farshchi *et al*. (2019) prepared CMC/Gel/TiO_2-Ag film through modifying carboxymethyl cellulose (CMC) with gelatin and TiO_2-Ag nanoparticles. The synthesized film improved the photocatalytic activity. Nair *et al*. (2020) improved light absorption and photocatalytic activity of cellulose nanocrystals (CNCs) by growing TiO_2 nanorods (NRs) on CNCs by an *in-situ* growth method. The above works mainly focused on the photocatalytic or antibacterial properties of composite materials or coatings prepared by nanocellulose or its derivatives modified by TiO_2. However, till now, changing the hydrophilia of nanocellulose coatings prepared by adopting TiO_2 to modify nanocellulose coatings has rarely been reported, especially cellulose nanowhiskers (CNWs) coating.

The objective of this paper was to change the hydrophilic character of CNWs coating by adopting TiO_2 to modify CNWs to have obtained the TiO_2/CNWs coating in a facile, eco-friendly fabrication method. Firstly, CNWs as the raw materials were modified with TiO_2 in pure water condition to form a newly homogeneous TiO_2/CNWs suspension. Thereafter, TiO_2/CNWs composite suspension was coated onto the glass slides by drop-coating method. The influence of adopting the different additive amount or particle size of TiO_2 to modify CNWs coating on the hydrophilia properties of CNWs coating was investigated. In addition, the chemical states and structures, crystallinity and morphology of modified and unmodified CNWs or CNWs coating were characterized.

EXPERIMENTAL

Materials

Cellulose nanowhiskers (CNWs) with 2% solid content were purchased from Northern Century (Jiangsu) Cellulose Materials Co., Ltd. (Jiangsu, China). The rutile titanium dioxide nanoparticles (TiO_2) with 30 nm diameters were provided by Dongguan Xinyu Chemical Co., Ltd. (Dongguan, China). The rutile titanium dioxide nanoparticles

(TiO_2) with 74 μm diameters were provided by Guangdong Puburn Nanotechnology Co. Ltd. (Shaoguan, China). Deionized water (DI) was prepared in the laboratory. Glass slides (7.5 cm × 2.5 cm) was purchased from Hebei Dingsheng Longhua Experimental Instrument Co., Ltd. (Shijiazhuang, China). Silicon sheet (23 mm × 23 mm) was provided by Harbin Tebo Technology Co., Ltd. (Harbin, China).

Synthesis

Preparation of the TiO_2/CNWs composite suspension

TiO_2 (74 μm) in different additive amounts (0.06 wt%, 0.1 wt%, 0.2 wt%, and 0.3 wt% with respect to the CNWs (2 wt%)) was added to deionized water to form 50 mL of suspension and dispersed by the ultrasonic cleaners for 30 min, which obtained different concentrations of TiO_2 dispersion. Four groups of 50 g of CNWs were separately combined with deionized water to form 100 mL of suspension and heated in a water bath under magnetic stirring. When they were heated to 70 ℃, the previously prepared different concentrations of TiO_2 dispersion were added into them by dripping slowly for 1 h. Subsequently, the obtained four groups of TiO_2/CNWs suspensions were magnetically stirred at 70 ℃ for 6 h. They continued to be stirred magnetically at room temperature for 12 h. In the end, the TiO_2/CNWs composite suspensions were obtained and were denoted as S-1, S-2, S-3, and S-4 respectively. The pristine CNWs suspension was prepared under the same conditions without the presence of TiO_2 and was denoted as S-0.

In addition, four groups of TiO_2/CNWs composite suspensions were prepared by changing TiO_2 particle size to 30 nm under the same conditions, where the additive quantity of TiO_2 were respectively 0.06 wt%, 0.1 wt%, 0.2 wt%, and 0.3 wt% relative to the CNWs (2 wt%), and were denoted as S-5, S-6, S-7, and S-8 respectively. The samples of S-0 and S-7 were vacuum-dried to obtain the solid contents of the suspensions for subsequent analysis and they were, respectively, denoted as CNWs and TiO_2/CNWs.

Preparation of the TiO_2/CNWs coating

The above CNWs suspension and eight groups of TiO_2/CNWs composite suspensions were respectively coated on glass slides by drop-coating method and dried at room temperature to obtain CNWs coating and TiO_2/CNWs coatings. Meanwhile, the obtained CNWs coating and eight groups of TiO_2/CNWs coatings were separately denoted as C-0, C-1, C-2, C-3, C-4, C-5, C-6, C-7, and C-8 correspond to the names of above suspensions. In the end, all coatings samples were used for subsequent analysis. All the above experimental samples are shown in Table 1.

Table 1. Experimental Samples

Suspension samples	Coating samples	TiO_2 (wt.%)	The particle size of TiO_2
S-0	C-0	0	---
S-1	C-1	0.06	74 μm
S-2	C-2	0.1	74 μm
S-3	C-3	0.2	74 μm
S-4	C-4	0.3	74 μm
S-5	C-5	0.06	30 nm
S-6	C-6	0.1	30 nm
S-7	C-7	0.2	30 nm
S-8	C-8	0.3	30 nm

Characterizations

Fourier infrared spectroscopy (FTIR) analysis

To analyze changes in chemical structures, an infrared spectrometer (Thermo Scientific Nicolet iS5, Massachusetts, USA) was used to obtain infrared spectrums of TiO_2, CNWs, and TiO_2/CNWs by the KBr pressed-disk technique. Before FTIR analysis, these samples were dried to eliminate the influence of the broad water peak. During the FTIR analysis, the background and every sample were scanned for 32 times at a speed of 0.2 cm/s from 400 to 4000 cm^{-1}. The resolution was set to 4 cm^{-1}.

Scanning electron microscopy (SEM) analysis

The topographies and surface microstructures of CNWs coating and TiO_2/CNWs coatings were explored with SEM (Zeiss Sigma 300, Jena, Germany). Prior to testing, the samples were cut into appropriate sizes and sprayed with a thin layer of gold.

Atomic force microscope (AFM) analysis

The morphologies of CNWs coating and TiO_2/CNWs coatings were studied by an AFM (Bruker Dimension Icon, Madison, USA). Before testing, the suspension of CNWs and TiO_2/CNWs were dripped onto two pieces of thin silicon sheet. They were dried at room temperature for the AFM measurement.

X-ray photoelectron spectroscopy (XPS) analysis

The elements and chemical states of CNWs and TiO_2/CNWs were measured by XPS (Escalab Xi+, Massachusetts, USA).

X-ray diffraction (XRD) analysis

An X-ray diffractometer (XD-2 diffractometer, Beijing Puxi Company, Beijing, China) was used to investigate the changes in the crystal structures between CNWs and TiO_2/CNWs. The instrument was equipped with CuKα radiation (λ=1.5406Å). The operating voltage was 40 kV, and the current was 300 mA. The data were collected within the 2θ range from 10° to 80° with a scan speed of 2°/min. The crystallinity index (Crt%) was obtained using Eq. 1,

$$\mathrm{Crt\%} = \frac{I_{200} - I_{\mathrm{am}}}{I_{200}} \cdot 100\% \quad (1)$$

where I_{200} represents the diffraction intensity of the (200) plane, and I_{am} is the amorphous area for minimum intensity between (110) and (200) plane (Dai *et al*. 2018).

Water contact angle (WCA) analysis

The water contact angles of CNWs coating and TiO_2/CNWs coatings were measured with a contact angle analyzer (Dataphysics DCAT21, Stuttgart, Germany). Samples were placed on a contact angle analyzer, and 5 μL of distilled water was dripped onto the surface of a sample. The contact angle between the water droplet and the sample surface was recorded. For each sample, the final contact angle value was the average value of three results obtained at three different places of the same sample surface.

RESULTS AND DISCUSSION

FTIR Spectroscopy Analysis

The FTIR physicochemical analysis of TiO_2, CNWs, and TiO_2/CNWs is illustrated in Fig. 1. For CNWs (Fig. 1b), a broad characteristic peak was seen at 3379 cm^{-1}, which indicates the stretching vibration of the O-H bond. The peak appearing at 1650 cm^{-1} is associated with the O-H bending of the adsorbed water. The peaks at 1429 and 1373 cm^{-1} are attributed to the bending vibration absorption of C-H bond of methyl and methylene, respectively. The peak appearing at 1061 cm^{-1} is associated with the stretching vibration of the C-O bond. The sharper and narrower peak appearing near 897 cm^{-1} is caused by the stretching vibration of the β-glucoside bond (Arularasu *et al*. 2020). Comparing with the spectra of CNWs, there was no other new characteristic absorption peak for TiO_2/CNWs (Fig. 1c), aside from two peaks at 423 cm^{-1} and 647 cm^{-1}, which are the characteristic absorbance peaks of TiO_2 (Fig. 1a) (Zhang *et al*. 2019). These results indicate that TiO_2 successfully was loaded on CNWs, but the addition of TiO_2 caused no significant chemical reaction with CNWs. TiO_2 was only physically dispersed in CNWs.

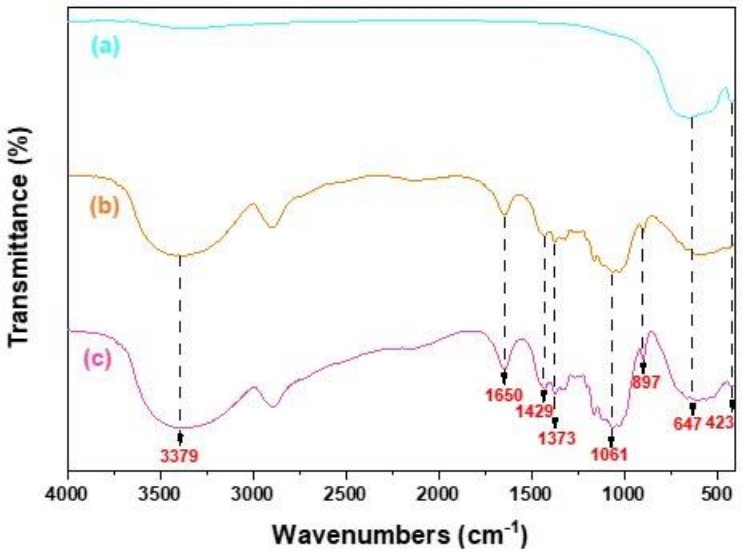

Fig. 1. FTIR spectra of (a) TiO_2, (b) CNWs and (c) TiO_2/CNWs

SEM Analysis

Figure 2 shows SEM images of C-0, C-3, and C-7. As shown in Fig. 2a, the surfaces of pure CNWs coating were very smooth and flat at low magnification.

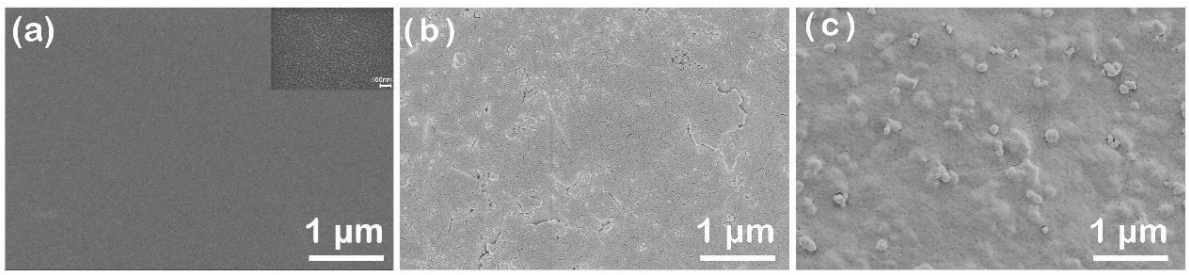

Fig. 2. SEM images of (a) C-0, C-3 and (b) C-7

It can be seen from Fig. 2b that TiO_2 particles were aggregated and the surface roughness of coating increased. Furthermore, the coating slightly cracked. However, in the surface morphology of C-7 (Fig. 2c), the TiO_2 particles are relatively evenly distributed in the coating. Most TiO_2 particles wrapped under the CNWs coating, and solely small amounts are exposed on the surface of the CNWs randomly. Moreover, the rough structure of coating was more obvious.

XPS Analysis

Figure 3a shows XPS spectra of the CNWs and TiO_2/CNWs and Fig. 3b shows the corresponding high-resolution spectra of O1s. Moreover, Table 2 provides the elemental contents analysis of the corresponding CNWs and TiO_2/CNWs.

Table 2. Elemental Contents of CNWs and TiO_2/CNWs

Samples	Elemental Contents		
	C (%)	O (%)	Ti (%)
CNWs	59.05	40.95	---
TiO_2/CNWs	57.58	41.76	0.65

As shown in Fig. 3(a), the characteristic signals of C1s and O1s correspond to 284.80 and 531.21 eV, respectively (Chen *et al*. 2020). In addition, very small characteristic signals of Ti2p correspond to 456.96 eV in TiO_2/CNWs (Pisarek *et al*. 2020). These results indicate that the addition of TiO_2 was very little. This is also demonstrated in Table 2. Comparing with CNWs, TiO_2/CNWs has an extra element of Ti which accounted for 0.65%. Moreover, Fig.3(b) exhibits the O1s spectrum of CNWs and TiO_2/CNWs. It can be observed that the main characteristic peaks corresponded to C-O-H (532.50 eV) (Eleutério *et al*. 2020) and C-O (531.51 eV) (Landoulsi *et al*. 2016) in CNWs, respectively. There is an additional characteristic peak correspond to Ti-O-Ti (529.16 eV) (Pisarek *et al*. 2020) in TiO_2/CNWs. But that chemical environment of O atoms had not changed. These findings indicate that TiO_2 was present in the organic system of CNWs by physical blending instead of chemical action. The result of analysis is consistent with the above-mentioned FTIR analysis.

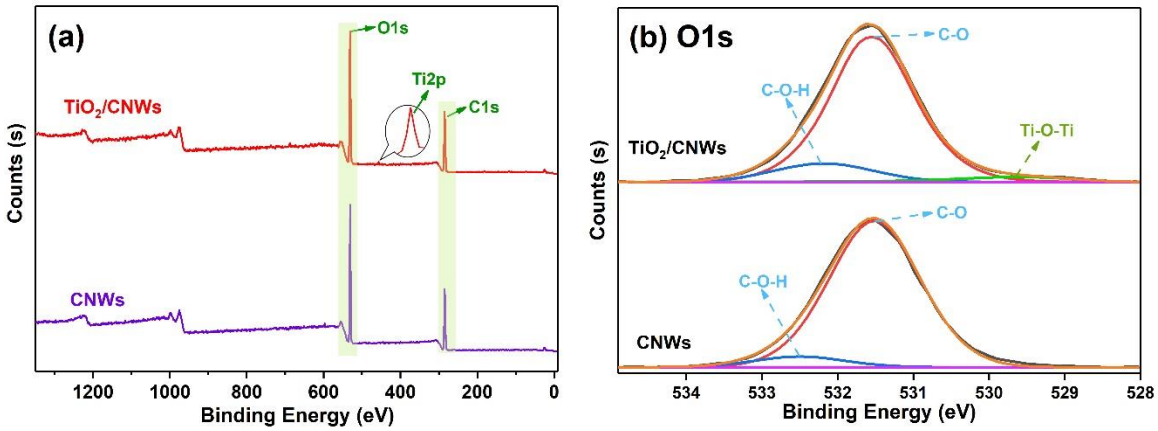

Fig. 3. (a)XPS spectra of CNWs and TiO_2/CNWs, (b) the corresponding high-resolution spectra of O1s

XRD Analysis

Figure 4 shows the XRD spectra of TiO_2, CNWs, and TiO_2/CNWs. Three strong diffraction peaks at 16.5°, 22.4°, and 34.4° in the XRD spectrum of the CNWs correspond to the (110), (200), and (004) planes, respectively, of cellulose crystals (Mhd Haniffa *et al*. 2017). As shown in the XRD spectrum of the TiO_2/CNWs, this sample retained the characteristic peaks of TiO_2 and CNWs. The two characteristic peaks of the CNWs were weakened in intensity, which may be attributed to the change in the amount of CNWs. These observations clearly indicate that TiO_2 physically combined with the CNWs. Because there were no chemical interactions between them, the TiO_2 did not change the CNWs physical characteristics. Using these XRD data, the crystallinity values of CNWs and TiO_2/CNWs were calculated as 79.67% and 84.89%, respectively. These data indicate that the addition of TiO_2 increased the crystallinity of CNWs.

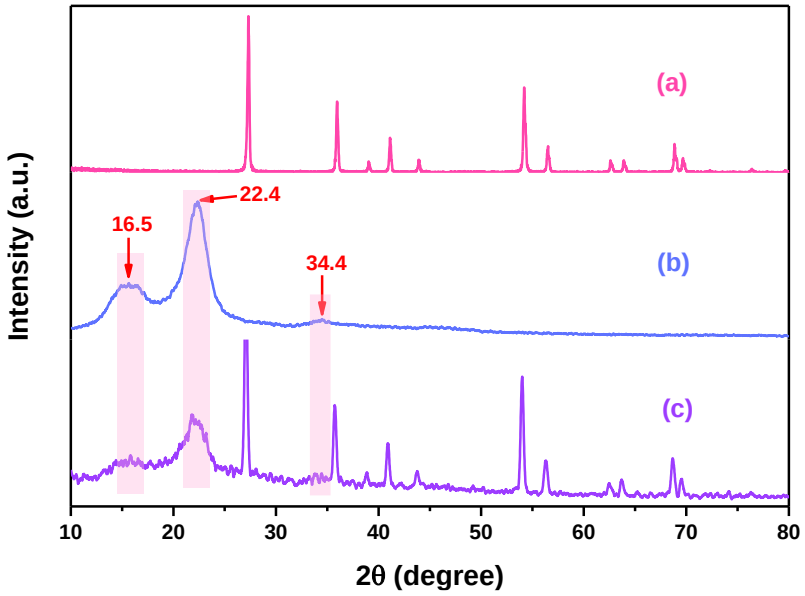

Fig. 4. XRD spectra of (a) TiO_2, (b) CNWs and (c) TiO_2/CNWs

AFM Analysis

Figure 5 shows AFM images of all coatings samples. The distribution of TiO_2 in the coating of each sample can be seen from these images. When the particle size of TiO_2 was 74 μm, the TiO_2 particles were evenly distributed in the coating with the increased addition of TiO_2 within the range of 0 to 0.1wt% (Fig.5a, 5b and 5c). However, when the additive amount of TiO_2 exceeded 0.1 wt%, the TiO_2 particles were unevenly distributed in the coating with the increased addition of TiO_2 (Fig.5d and 5e). The distribution of 30 nm TiO_2 seemed to be similar to74 μm TiO_2, whereas the additive amount of TiO_2 exceeded 0.2 wt% began to unevenly distribute (Fig.5f, 5g, 5h, and 5i). In addition, comparing with 74 μm TiO_2, 30 nm TiO_2 was relatively uniformly distributed in the coating. This may be attributed to the tendency for excessive TiO_2 particles to aggregate (Garusinghe *et al*. 2018) and the larger particle size led to more aggregation, which is in line with the above-mentioned SEM analysis.

Furthermore, it can be seen from Fig. 5 that the addition of TiO_2 affected the surface roughness (R_q) of the CNWs coating. According to the data of R_q obtained by analysis, the relation curves of R_q changing with the increased addition of TiO_2 were drawn in Fig. 6.

Fig. 5 and 6 indicated that the addition of TiO_2 led to increase the roughness of coating. As shown in Fig. 5 and Fig. 6(a), when the particle size of TiO_2 was 30 nm, the coatings were present as micro-nanoscale mastoid structures. Moreover, the R_q of the TiO_2/CNWs coating increased with the increased addition of TiO_2 within the range of 0 to 0.2 wt%; however it decreased with the increased addition of TiO_2 within the range of 0.2 to 0.3 wt%. When the additive amount of TiO_2 was 0.2 wt%, the R_q of the TiO_2/CNWs coating reached the maximum (135 nm).

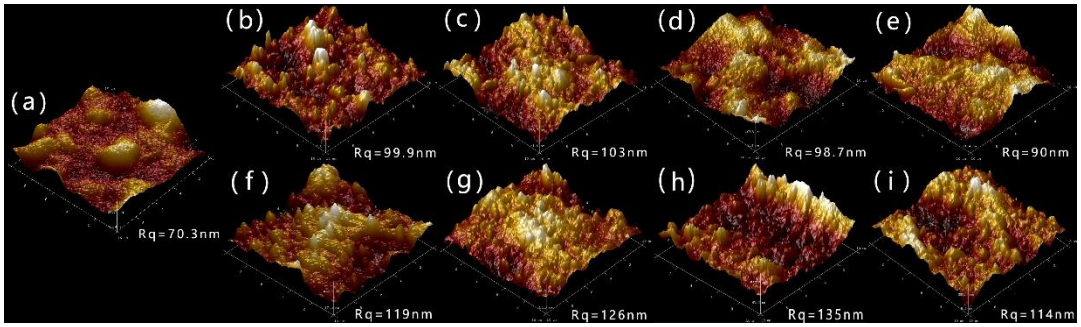

Fig. 5. AFM images of (a) C-0, (b) C-1, (c) C-2, (d) C-3, (e) C-4, (f) C-5, (g) C-6, (h) C-7, and (i) C-8

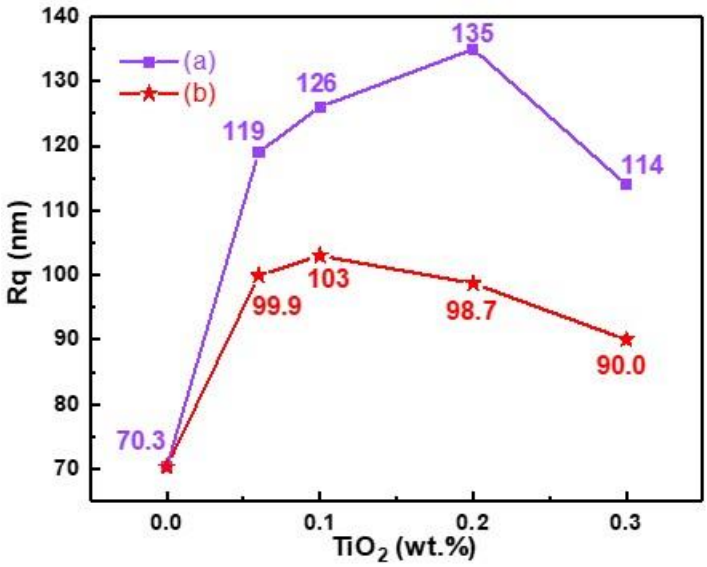

Fig. 6. Influence of different additive amounts of (a) TiO_2 (30 nm) and (b) TiO_2 (74 μm) on the R_q of the TiO_2/CNWs coating

As shown in Fig. 5 and Fig. 6(b), when the particle size of TiO_2 was 74 μm, the micro-nanoscale mastoid structures also can be found in C-1 and C-2. However, other coatings only existed as a nanoscale structure. Moreover, the R_q of the TiO_2/CNWs coating increased with the increased addition of TiO_2 at the range of 0 to 0.1 wt%; however it decreased with the increased addition of TiO_2 within the range of 0.1 to 0.3 wt%. When the additive amount of TiO_2 was 0.1 wt%, the R_q of the TiO_2/CNWs coating reached the maximum (103 nm). In addition, when the additive amount of TiO_2 was the same, the R_q of the TiO_2/CNWs coating prepared by TiO_2 (30 nm) was higher than TiO_2 (74 μm). For example, the R_q of C-7 (135 nm) was higher than that of C-3 (97.8 nm), which is in line

with the above-mentioned SEM analysis. Therefore, the additive amount and particle size of TiO_2 can affect the R_q of the TiO_2/CNWs coating, which may be attributed to that most TiO_2 evenly distributed and was wrapped under the surface of the CNWs coating when the addition dosage of TiO_2 was small, so the R_q increased slightly. With the further increase of TiO_2, different concave-convex structure was formed, so the R_q continued to increase. However, excessive TiO_2 led to aggregates, which could not be completely wrapped under the surface of the coating. Meanwhile, the coating cracked and finally the R_q decreased (Wu *et al*. 2019).

Water Contact Angle Analysis

The hydrophilicity characteristics of all coating samples were assessed based on their water contact angles. When the particle size of TiO_2 was 30 nm or 74 μm, the results of the influence of different additive amounts of TiO_2 on the WCA of the TiO_2/CNWs coating are shown in Fig. 7. The images of the WCA of C-0, C-3, and C-7 are shown in Fig. 8.

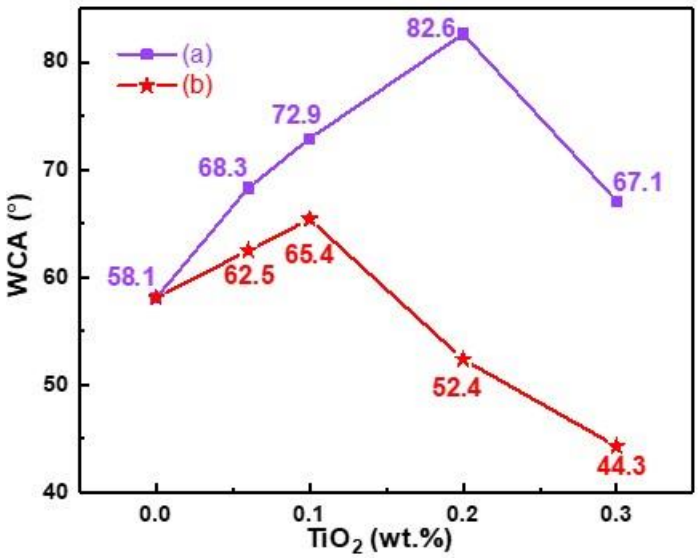

Fig. 7. Influence of different additive amounts of (a)TiO_2 (30 nm) and (b) TiO_2 (74 μm) on the WCA of the TiO_2/CNWs coating

When a water droplet was placed on the CNWs coating, the water droplet spread immediately and penetrated the inside of the coating, resulting in softening of the CNWs coating. The WCA of the CNWs coating was 58.1° (Fig. 8a), which implies that the CNWs coating is hydrophilic and can be easily destroyed by aqueous solutions. As shown in Fig. 7(a), when the particle size of TiO_2 was 30 nm, the WCA of the TiO_2/CNWs coating increased with the increased addition of TiO_2 within the range of 0 to 0.2 wt%; however it decreased with the increased addition of TiO_2 within the range of 0.2 to 0.3 wt%. When the additive amount of TiO_2 was 0.2 wt%, the WCA of the TiO_2/CNWs coating reached a maximum, which means that the hydrophilicity was at a minimum. Meanwhile, the WCA of all TiO_2/CNWs coating was higher than the CNWs coating. The variation trend of the WCA was the same as for the R_q of the coating in the AFM analysis. This may be attributed to the surface formed the micro-nanoscale mastoid structures. A hierarchical surface roughness makes the surface more hydrophobic than that a nonhierarchical roughness. Owing to the hydrophilic nature of the surface of TiO_2/CNWs coating, however, the

droplets on the surfaces with hierarchical roughnesses ending up being in the Wenzel states (Kwon *et al.* 2018). As shown in Fig. 7(b), when the particle size of TiO_2 was 74 μm, adding TiO_2 to the CNWs coating can change the WCA of the CNWs coating. The WCA of the TiO_2/CNWs coating increased with the increased addition of TiO_2 within the range of 0 to 0.1 wt% and they were higher than the CNWs coating; however it decreased with the increased addition of TiO_2 at the range of 0.1 to 0.3 wt% and they were lower than the CNWs coating, which may be attributed to the surface of C-3 and C-4 only forming the nanoscale roughness, so the surface of coating remains Wenzel state and finally increased the roughness led to increase of hydrophilicity. When the additive amount of TiO_2 was 0.1 wt%, the WCA of the TiO_2/CNWs coating reached a maximum, meaning that the hydrophilicity was at a minimum. The variation trend of the WCA was the same as for the R_q of the coating in the AFM analysis. In addition, when the additive amount of TiO_2 was the same, the WCA of the TiO_2/CNWs coating prepared by TiO_2 (30 nm) was higher than that of TiO_2 (74 μm). For example, when the additive amount of TiO_2 was 0.2 wt.%, the particle size of TiO_2 was 30 nm, the WCA of the obtained C-7 was 82.1° (Fig. 8c). However, when the particle size of TiO_2 was 74 μm, the WCA of the obtained C-3 was 52.4° (Fig. 8b). Meanwhile, the WCA of C-7 was maximized in all samples. The results are consistent with that of R_q of the coating in the AFM analysis. The above results indicated that the changes of the hydrophilia of the obtained TiO_2/CNWs coating might be attributed to the changes in the R_q of the coating, the distribution of TiO_2 in the coating and integrity of the coating, as well as the forming the micro-nanoscale mastoid structures. Therefore, changing the additive amount and particle size of TiO_2 can change the hydrophilia of the obtained TiO_2/CNWs coating.

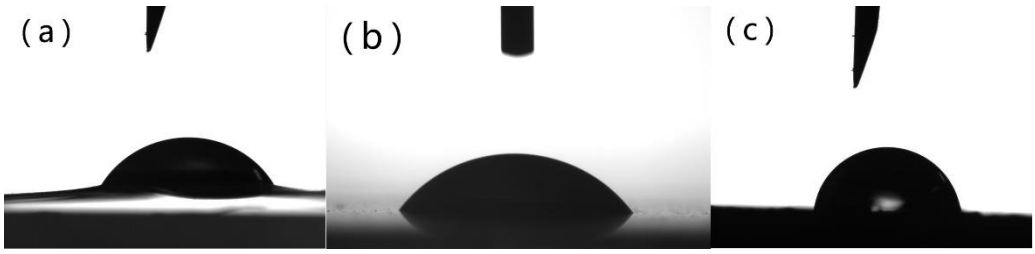

Fig. 8. Images of the WCA of (a) C-0, (b) C-3, and (c) C-7

CONCLUSIONS

1. Coating materials comprised of titanium dioxide particles and cellulose nanowhiskers (TiO_2/CNWs) were successfully formed by adopting TiO_2 to modify CNWs.
2. Different additive amounts and particle sizes of TiO_2 were found to have different effects on the surface structure and the water contact angle (WCA) of the coatings that is say the hydrophilic of the coatings. The hydrophilic character of the obtained TiO_2/CNWs coating was affected by the R_q of the coating, the distribution of TiO_2 in the coating, integrity of the coating, as well as the forming the micro-nanoscale mastoid structures. In addition, when the particle size of TiO_2 was 30 nm and the additive amount of TiO_2 was 0.2 wt%, the TiO_2 particles were relatively evenly distributed in obtained TiO_2/CNWs coating and formed the micro-nanoscale roughness structures, the Rq of the coating reached the maximum and was 135 nm, as well as the WCA of

the coating reached the maximum and was 82.1°, meaning that the hydrophilicity was at a minimum.

3. The results of XRD exhibited that the addition of TiO_2 improved the crystallinity of CNWs from 79.67% to 84.89%.
4. The FTIR and XPS results confirmed that TiO_2 was only physically dispersed in CNWs instead of having significant chemical reaction with CNWs.

ACKNOWLEDGMENTS

The authors are grateful for the support of the Key Project of Education Department of Hunan Province, Grant No.19A521 and the Special Project of Department of Science and Technology of Guangdong Province, Grant No. GDKTP2020019900.

Conflicts of Interest

There is no conflict to declare.

REFERENCES CITED

Abitbol, T., Rivkin, A., Cao, Y., Nevo, Y., Abraham, E., Ben-Shalom, T., Lapidot, S., and Shoseyov, O. (2016). "Nanocellulose, a tiny fiber with huge applications," *Curr. Opin. Biotechnol.* 39, 76-88. DOI: 10.1016/j.copbio.2016.01.002

Ahmed, A., Adak, B., Bansala, T., and Mukhopadhyay, S. (2020). "Green solvent processed cellulose/graphene oxide nanocomposite films with superior mechanical, thermal, and ultraviolet shielding properties," *ACS Appl. Mater. Inter.* 12(1), 1687-1697. DOI: 10.1021/acsami.9b19686

Ali, I., Suhail, M., Alothman, Z. A., and Alwarthan, A. (2018). "Recent advances in syntheses, properties and applications of TiO_2 nanostructures," *RSC Adv.* 8, 30125-30147. DOI: 10.1039/c8ra06517a

Arularasu, M. V., Harb, M., and Sundaram, R. (2020). "Synthesis and characterization of cellulose/TiO_2 nanocomposite: Evaluation of in vitro antibacterial and in silico molecular docking studies," *Carbohydr. Polym.* 249, 116868. DOI: 10.1016/j.carbpol.2020.116868

Borsoi, C., Zimmernnam, M. V. G., Zattera, A. J., Santana, R. M. C., and Ferreira, C. A. (2016). "Thermal degradation behavior of cellulose nanofibers and nanowhiskers," *J. Therm. Anal. Calorim.* 126, 1867-1878. DOI: 10.1007/s10973-016-5653-x

Chen, Q. F., Xiong, J. Y., Chen, G. X., and Tan, T. Y. (2020). "Preparation and characterization of highly transparent hydrophobic nanocellulose film using corn husks as main material," *Int. J. Biol. Macromol.* 158, 781-789. DOI: 10.1016/j.ijbiomac.2020.04.250

Čolić, M., Tomić, S., and Bekić, M. (2020). "Immunological aspects of nanocellulose," *Immunol. Lett.* 222, 80-89. DOI: 10.1016/j.imlet.2020.04.004.

Dai, H., Ou, S., Huang, Y., and Huang, H. H. (2018). "Utilization of pineapple peel for production of nanocellulose and film application," *Cellulose* 25, 1743-1756. DOI: 10.1007/s10570-018-1671-0

Eleutério, T., Sério, S., Teodoro, O. M. N. D., Bundaleski, N., and Vasconcelos, H. C.

(2020). "XPS and FTIR studies of DC reactive magnetron sputtered TiO_2 thin films on natural based-cellulose fibers," *Coatings* 10(3), 287. DOI: 10.3390/coatings10030287

Farshchi, E., Pirsa, S., Roufegarinejad L., Alizadeh, M., and Rezazad, M. (2019). "Photocatalytic/biodegradable film based on carboxymethyl cellulose, modified by gelatin and TiO_2-Ag nanoparticles," *Carbohydr. Polym.*, 216, 189-196. DOI: 10.1016/j.carbpol.2019.03.094

Galkina, O. (2015). Functional hybrid bionanomaterials based on titanium dioxide and cellulose, possessing antibacterial and drug delivery properties, Licentiate Thesis, Swedish University of Agricultural Sciences, Uppsala, Sweden.

Garusinghe, U. M., Raghuwanshi, V. S., Batchelor, W., and Garnier, G. (2018). "Water resistant cellulose - titanium dioxide composites for photocatalysis. *Sci. Rep.* 8, 2306. DOI:10.1038/s41598-018-20569-w

Herrera, M. A., Mathew, A. P., and Oksman, K. (2017). "Barrier and mechanical properties of plasticized and cross-linked nanocellulose coatings for paper packaging applications," *Cellulose*. 24, 3969-3980. DOI: 10.1007/s10570-017-1405-8

Hubbe, M. A., Ferrer, A., Tyagi, P., Yin, Y. Y., Salas, C., Pal, L., and Rojas, O. J. (2017). "Nanocellulose in thin films, coatings, and plies for packaging applications: a review," *BioResources* 12(1), 2143-2233. DOI: 10.15376/biores.12.1.2143-2233

Huang, J. D., Lyu, S. Y., Chen, Z. L., Wang, S. Q., and Fu, F. (2019). "A facile method for fabricating robust cellulose nanocrystal/SiO_2 superhydrophobic coatings," *Colloid Interface Sci.* 536, 349-362. DOI: 10.1016/j.jcis.2018.10.045

Kettunen, M., Silvennoinen, R. J., Houbenov, N., Nykänen, A., Ruokolainen, J., Sainio, J., Pore, V., Kemell, M., Ankerfors, M., Lindström, T., Ritala, M., Ras, R. H. A., and Ikkala, O. (2010). "Photoswitchable superabsorbency based on nanocellulose aerogels," *Adv. Funct. Mater.* 21(3), 510-517. DOI: 10.1002/adfm.201001431

Koppolu, R., Lahti, J., Abitbol, T., Swerin, A., Kuusipalo, J., and Toivakka, M. (2019). "Continuous processing of nanocellulose and polylactic acid into multilayer barrier coatings," *ACS Appl. Mater. Inter.* 11(12), 11920-11927. DOI: 10.1021/acsami.9b00922

Kwon, T. W., Jang, J., Ambrosia, M. S., and Ha, M.Y. (2018). "Molecular dynamics study on the hydrophobicity of asurface patterned with hierarchical nanotextures," *Colloid Surface A.* 559, 209-217. DOI:10.1016/j.colsurfa.2018.09.056

Mhd Haniffa, M. A. C., Ching, Y. C., Chuah, C. H., Yong Ching, K., Nazri, N., Abdullah, L. C., and Nai-Shang, L. (2017). "Effect of TEMPO-oxidization and rapid cooling on thermo-structural properties of nanocellulose," *Carbohydr. Polym.* 173, 91-99. DOI: 10.1016/j.carbpol.2017.05.084

Nair, S. S., Chen, J. H., Slabon, A., and Mathew, A. P. (2020). "Converting cellulose nanocrystals into photocatalysts by functionalisation with titanium dioxide nanorods and gold nanocrystals," *RSC Adv.* 10(61), 37374-37381. DOI: 10.1039/D0RA05961G

Neelapala, S. D., Nair, A. K., and Jagadeesh Babu, P. E. (2017). "Synthesis and characterisation of TiO_2 nanofibre/cellulose acetate nanocomposite ultrafiltration membrane," *Exp. Nanosci.* 12(1), 152-165. DOI: 10.1080/17458080.2017.1285446

Nguyen, L. H., Naficy, S., Chandrawati, R., and Dehghani, F. (2019). "Nanocellulose for sensing applications," *Adv. Mater. Interfaces* 6(18), 1900424. DOI: 10.1002/admi.201900424

Landoulsi, J., Genet, M. J., Fleith, S., Touré, Y., Liascukiene, I., Méthivier, C., and Rouxhet, P. G. (2016). "Organic adlayer on inorganic materials: XPS analysis

selectivity to cope with adventitious contamination," *Appl. Surf. Sci.* 383, 71-83. DOI: 10.1016/j.apsusc.2016.04.147

Lu, J. P., Chen, L. and Song, R. G. (2018). "Effects of SiO_2 particle size on the corrosion resistance of fluoropolymer/SiO_2 composite coatings," *Sur. Eng.* 35(5), 440-490. DOI:10.1080/02670844.2018.1491511

Pisarek, M., Krawczyk, M., Hołdyński, M., and Lisowski, W. (2020). "Plasma nitriding of TiO_2 nanotubes: N-Doping in situ investigations using XPS," *ACS Omega* 5(15), 8647-8658. DOI: 10.1021/acsomega.0c00094

Rathod, M., Moradeeya, P. G., Haldar, S., and Basha, S. (2018). "Nanocellulose/TiO_2 composites: Preparation, characterization and application in photocatalytic degradation of a potential endocrine disruptor, mefanamic acid, from aqueous media," *Photochem. Photobiol. Sci.* 17(10): 1301-1309. DOI: 10.1039/C8PP00156A

Schütz, C., Sort, J., Bacsik, Z., Oliynyk, V., Pellicer, E., Fall, A., Wågberg, L., Berglund, L., Bergström, L., and Salazar-Alvarez, G. (2012). "Hard and transparent films formed by nanocellulose-TiO_2 nanoparticle hybrids," *PLoS One* 7(10): e45828. DOI: 10.1371/journal.pone.0045828

Shi, S. C., Wang, C. C., Cheng, Y. C., and Lin, Y. F. (2020). "Surface characterization and tribological behavior of graphene-reinforced cellulose composites prepared by large-area spray coating on flexible substrate," *Coatings* 10(12), 1176. DOI: 10.3390/coatings10121176

Song, J. L., and Rojas, O. J. (2013). "Approaching super-hydrophobicity from cellulosic materials: A Review," *Nord. Pulp Pap. Res. J.* 28(2), 216-238. DOI: 10.3183/npprj-2013-28-02-p216-238

Su, Y. Y., Li, K. Z., Zhang, L. L., Wang, C. C., and Zhang, Y. P. (2018). "Effect of the hydroxyapatite particle size on the properties of sprayed coating," *S.C.T.* 352, 619-626. DOI:10.1016/j.surfcoat.2018.08.052

Tortorella, S., Vetri Buratti, V., Maturi, M., Sambri, L., Comes Franchini, M., and Locatelli, E. (2020). "Surface-modified nanocellulose for application in biomedical engineering and nanomedicine: A review," *Int. J. Nanomedicine* 15, 9909-9937. DOI: 10.2147/ijn.s266103

Wang, X., Liu, F., Li, Y. D., Zhang, W. B., Bai, S. W., Zheng, X. L., Huan J. M, Cao G. L., Yang, T. H., Wang, M., Jiang, Z. S., Wang, C. Y., and Ho, S. H. (2020). "Development of a facile and bi-functional superhydrophobic suspension and its applications as superhydrophobic coating and aerogel in high-efficiency oil-water separation," *Green Chem.* 22, 7424-7434. DOI: 10.1039/d0gc01834a

Wu, G. M., Liu, D., Chen, J., Liu, G. F., Kong, Z. W. (2019). "Preparation and properties of super hydrophobicfilms from siloxane-modified two-component waterborne polyurethane and hydrophobic nano SiO_2," *Prog. Org. Coat.*127, 80-87. DOI: 10.1016/j.porgcoat.2018.06.016

Xue, Y., Mou, Z. H., and Xiao, H. N. (2017). "Nanocellulose as sustainable biomass material: Structure, properties, present status and future prospects in biomedical applications," *Nanoscale* 9, 14758-14781. DOI: 10.1039/c7nr04994c

Zhang, C., Uchikoshi, T., Ichinose, I., and Liu, L. (2019). "Surface modification on cellulose nanofibers by TiO_2 coating for achieving high capture efficiency of nanoparticles," *Coatings* 9(2),139. DOI: 10.3390/coatings9020139

Zheng, X. M., and Fu, S. Y. (2019). "Reconstructing micro/nano hierarchical structures particle with nanocellulose for superhydrophobic coatings," *Colloid Surface A* 560, 171-179. DOI: 10.1016/j.colsurfa.2018.10.005

Zinge, C., and Kandasubramanian, B. (2020). "Nanocellulose based biodegradable polymers," *Eur. Polym. J.* 133, 109758. DOI: 10.1016/j.eurpolymj.2020.109758

Zuo, K., Wu, J., Chen, S., Ji, X. X., and Wu, W. B. (2019). "Superamphiphobic nanocellulose aerogels loaded with silica nanoparticles," *Cellulose* 26, 9661-9671. DOI: 10.1007/s10570-019-02774-6

Article submitted: June 19, 2021; Peer review completed: July 17, 2021; Revised version received: October 29, 2021; Further revised versions received: November 6, 20, and 21, 2021; Article accepted: November 21, 2021; Published: November 24, 2021.
DOI: 10.15376/biores.17.1.504-518